ISSN: 0974-5823 Vol. 6 No. 3 October-December, 2021

International Journal of Mechanical Engineering

$BaCoO_{3-\delta}$ semiconductor preparation using heterometallic Ba-Co carbonate precursor

P. Hariharan*
Department of Biotechnology, PSG College of Technology, Coimbatore, Tamil Nadu, India.
Email: hariharan685@gmail.com; phh.bio@psgtech.ac.in

K. Agilandeswari
Department of Chemistry, PSG College of Arts & Science, Coimbatore, Tamil Nadu, India.

Abstract

The co-precipitation carbonate precursor process was used to make $BaCoO_{3-\delta}$ ceramic. The phase formation temperature of $BaCoO_{3-\delta}$ is 900°C, according to thermogravimetric and differential thermal analysis (TGA-DTA). Powder X-ray diffraction (XRD) was used to describe the product, which revealed the monoclinic structure of single phase $BaCoO_{3-\delta}$. Using the higher and lower frequency absorption bands of $BaCoO_{3-\delta}$ were discovered by using Fourier transform infrared spectroscopy (FTIR) and FT-Raman spectroscopy. Images taken with a high-resolution scanning electron microscope (HRSEM) showed the rod-shaped barium carbonate precursor transforms into a sphere-shaped oxide result. Energy Dispersive X-ray analysis (EDX) was used to determine the chemical composition and purity of $BaCoO_{3-\delta}$. Optical absorption experiments using UV-Visible Diffuse Reflectance Spectroscopy (DRS) reveal the barium cobalt carbonate precursor as an insulating material and the $BaCoO_{3-\delta}$ as semiconducting. The carbonate precursor is paramagnetic, whereas its oxide $BaCoO_{3-\delta}$ is superparamagnetic, according to a room temperature magnetic investigation. The space charge polarization mechanism is used in the dielectric study to establish the conduction behavior of the precursor and oxide.

Keywords: Oxides, Semiconductors, Co-precipitation, Magnetic property.

1. Introduction

The oxygen defect structure in perovskites is of great interest because of its many properties, including electrical, magnetic, and superconductivity, as well as its role as a catalyst for pollutant degradation. The production and dispersion of oxygen vacancies in the perovskite during a redox reaction, often at high temperatures, is the basis for energy applications[1]. The semiconducting perovskite oxide $BaCoO_{3-\delta}$ material's most essential feature. Reduced cations Co^{3+} (d^6) are present in the octahedral coordination while Co^{4+} (d^5) is present in both the tetrahedral and octahedral sites in the $BaCoO_{3-\delta}$ layer structure. $BaCoO_{3-\delta}$ can take on a variety of phases depending on partial oxygen pressures, including 2H – perovskite structure with $BaCoO_{2.94}$, 5H, and 12H layer structure[2]–[4] Beatrice et al. were the first to describe a single crystal of $BaCoO_{3-\delta}$, although preparing the compound with this flux approach takes a lengthy time. However, there are more disadvantages in the solid form, such as high reaction temperatures, limited chemical homogeneity, and a long process time. Preparing $BaCoO_{3-\delta}$ using a citrate sol-gel approach resulted in higher temperatures and poorer uniformity [5]–[7]. The wet-chemical method has several advantages, including excellent mixing of the initial components, which results in high chemical homogeneity in the final product. Moreover, $BaCo_{0.8}Al_{0.2}O_3$ has strong cyclic reactivity and stability, and can offer a stable O_2/CO_2 mixed gas for a variety of applications oxy-fuel combustion [8][9]. At a lower temperature, the development of a $BaSc_{0.25}Co_{0.75}O_{3-\delta}$ cathode component with high oxygen reduction reaction (ORR) activity[10].

Novel air-electrode materials based on $BaCoO_3$ perovskites adorned with socketed Ag nanoparticles inspired by recent achievements. Niobium (Nb^{5+}) and tantalum (Ta^{5+}) doping can improve the stability of the cubic perovskite phase[1].The solid solution carbonate precursor method for preparing $BaCoO_{3-\delta}$ is discussed in this research. During the precipitation process, divalent Co^{2+} cations are incorporated into barium carbonate (witherite mineral name). A distribution coefficient for Ba^{2+} from an aqueous solution into Cobalt carbonate (spherocobaltite) in calcite structure was reported by the researchers. The physiochemical circumstances of precipitate generation influence crystallization [11]–[13]. The orthorhombic crystal structure generated during the precipitation synthesis of the whitherite form of $BaCo(CO_3)_2$. $BaCoO_{3-\delta}$ was formed from the carbonate precursor. $BaCoO_{3-\delta}$ has yet to be discovered using this precursor technique. In comparison to other ceramic processes, the advantage of the precursor method is that the metals ratio is maintained in a homogeneous form. The rod-shaped carbonate precursor and sphere-shaped oxide result are visible in SEM micrographs. It displays the precursor as an insulating material and the $BaCoO_{3-\delta}$ as a semiconducting material in terms of optical band gap. The carbonate precursor is paramagnetic, whereas its oxide $BaCoO_{3-\delta}$ is superparamagnetic, according to a room temperature magnetic investigation.

2. Experimental

2.1. Preparation of $BaCoO_{3-\delta}$ by carbonate precursor method:

Cobalt nitrate and barium nitrate stoichiometry ratios were dissolved in deionized water at 80°C with continual stirring. 2M sodium carbonate was dripped into the combined salt solution as a precipitating agent, stirring gently until the pH of the salt solution reached 8.5. The precipitated carbonate was mixed for 0.5 hours to achieve homogeneity, then washed with distilled water and dried for 4 hours at 100°C. The colorless filtrate was put to the test to see if it had precipitated completely. The acquired barium cobalt carbonate (Witherite mineral – purple colour) precursor can then be decomposed at 900°C for 3 hours in the presence of air, yielding single phase $BaCoO_{3-\delta}$

2.2. Characterization Technique

SDT Q600 V20.9 model was used to perform a thermographic differential thermal investigation of the precursor and oxide material. X-ray diffraction (XRD, Bruker D8 Advance, CuK radiation, k = 1.5406) was used to characterize the powders. A JASCO 400 infrared spectrometer was used to study FTIR spectrums. A scanning electron microscope was used to examine the surface morphology and microstructure (HRSEM FEI Inspect F50). An EDX analyzer connected to a (HRSEM FEI Inspect F50) device was used to determine the chemical composition. Jasco V-670-UV-Visible diffused reflectance spectrometer was used to determine the optical band gap. VSM examined the magnetic characteristics (Lakeshore VSM 7410). LCR meter (HIOKI 3532-50 LCR meter HITESTER) in the frequency range from 50Hz to 5MHz was carried conducted dielectric investigations.

3. Results and discussion

The thermal analysis of barium cobalt carbonate precursor is shown in Figure 1. TGA-DTA was used to analyze the decomposition mechanism of carbonate precursors and product forms. Thermal analysis was carried out in an oxygen environment at a rate of 4°C/min from ambient temperature to 950°C. Due to the evaporation of leftover water, the endothermic peak at 183°C results in a modest weight loss. At 212°C, one molecule of carbon dioxide is lost, followed by the formation of oxycarbonates. When the temperature is raised to 730°C, a minor endothermic peak appears, revealing the breakdown of oxycarbonate to oxide. At a temperature of 900°C, the stable $BaCoO_{3-\delta}$ product formed. The product production is proven by the overall weight reduction of 23.49% and the phase identification done by XRD.

Plausible stepwise decompositions

Step-1 $BaCo(CO_3)_2 \xrightarrow[250\text{-}650°C]{O_2} BaCoO(CO_3) + CO_2$

Step-2 $BaCoO(CO_3) \xrightarrow[800\text{-}900\,°C]{O_2} BaCoO_{3-\delta} + CO_2$

Overall decomposition step

$$\mathbf{BaCo(CO_3)_2} \xrightarrow{900\,°C} \mathbf{BaCoO_{3-\delta} + 2CO_2}$$

(purple color) **(black color)**

Figure 2 shows the XRD pattern of the product after being calcined for 2 hours at 250-900°C. The BaCO3 phase was found after 2 hours of calcination at 250-650°C. When barium carbonate is heated to 800°C for 2 hours, it decomposes into a mixed phase of BaCO3 and Co3O4. When the temperature is raised to 900°C, the XRD pattern reveals that the BaCoO3-δ single phase has formed into a hexagonal system with lattice parameters a =b=5.6831 and c =4.7183 that are compatible with those published in JCPDS (card No 01-070-0363). The Scherer equation was used to determine the crystallite sizes of samples. [8].

$$D= K\lambda/\beta cos\theta \qquad (1)$$

K is the so-called shape factor, D is the crystallite size (nm); X-ray wavelength which is usually around 0.9. To calculate the average crystallite size of 400nm, the most intense (101) plane of $BaCoO_{3-\delta}$ was used for the crystal size analysis.

Figure 3 shows a SEM image of $BaCo(CO_3)_2$ carbonate precursor and $BaCoO_{3-\delta}$ particles created utilizing the carbonate precursor method. A variety of magnifications are depicted in the figures. The material has a micro porous combined rod like morphology to investigate the morphology evolution of the precursor samples, and the product oxide samples have a micro porous spherical plate like morphology composed of agglomerated spheres of different grains with good connectivity between the grains. The EDX pattern verifies the XRD findings and reveals the B $aCoO_{3-\delta}$ composition.

By capturing a component of the SEM image in the form of peaks, Figure 4 shows how to utilize EDX to measure the elements in the sample that has been prepared. FTIR spectra of the carbonate precursor and its degraded products at various temperatures are shown in Figure. 5. The large peak at 3480 and 1630cm^{-1} in the carbonate precursor produced at 100°C can be attributed to absorbed water, while 1435cm-1 indicates the witherite carbonate mineral [9]. When the precursor is calcined at 250°C, two bands appear at 1435 and 860cm-1, which are attributable to the stretching vibration of the carbonate peak. When the carbonate decomposes from the spectra at 800°C, the peak intensity of the bands at 1440 and 850cm-1 decreases. The bands occur at 730cm-1, 570cm-1, and 469cm-1 after calcination at 900°C due to asymmetric stretching vibrations of Ba-O and Co-O bonds. [14].

FT-Raman spectra for the barium cobalt carbonate precursor recorded in KBr matrix shows a large peak at 3085cm^{-1} and 1065cm^{-1}, which corresponds to the witherite carbonate mineral[15]. Due to the synthesis of Ba-O and Co-O groups, the oxide product $BaCoO_{3-\delta}$ occurred at ($A1_g$) 682cm^{-1} and (E_g) 475cm^{-1}.

At room temperature, Fig.7 depicts reflectance spectra between 200 and 1000 nm wavelength areas, which are identical to absorbance spectra. Use Tauc's connection in equation to calculate a sample's optical band gap (2)

$$(\alpha h\upsilon)^n = A(h\upsilon - E_g) \qquad (2)$$

The absorption coefficient is represented by the letters A, E_g, and n, where A represents the constant, E_g represents the band gap, and n represents the exponent, which varies depending on the kind of transition. The optical band gap is obtained by plotting $(\alpha hv)^2$ against hγ, where and denote the absorption coefficient and photon energy, respectively, and projecting the curve to the photon energy axis using the Tauc relation. As illustrated in Fig.8, the band-gap energy (E_g) values were calculated using Tauc's plot.

UV-Visible DRS absorption spectra were used to investigate the optical band gap parameters of barium cobalt carbonate precursor and $BaCoO_{3-\delta}$ oxide product. Because of ligand to metal charge transfer (LMCT) from O^{2-} to octahedral Co^{2+}, the optical absorption plot of carbonate precursor exhibits a broad energy band gap of 4eV, confirming the insulating feature. Cobalt charge transfer from O2- to mixed oxidation state as a result of ligand to metal charge transfer of (Co^{2+} & Co^{3+}) at 2eV, the optical absorption band gap of the oxide product. As a result, the barium cobalt oxide system exhibits semiconducting behavior when d-d charge transfer occurs.

A Vibrating Sample Magnetometer was used to assess the room temperature magnetic characteristics of barium cobalt carbonate precursor and oxide product (VSM). At room temperature, the graph depicted the magnetic moment vs. applied magnetic field.

Table 1 shows the magnetic properties of the synthesized barium cobalt carbonate (witherite) precursor and $BaCoO_{3-\delta}$ oxide. Both the carbonate precursor and the oxide substance are found to be paramagnetic. The carbonate precursor's magnetic retentivity remains unchanged, but the magnetic saturation moment increases due to the reduction in domain size. Due to the presence of cobalt in a single Co2+ oxidation state, the external field coercivity of barium cobalt carbonate precursor is double that of oxide. Carbonate to oxide materials that are anisotropic have their moment aligned in one direction of spontaneous magnetization and exhibit superparamagnetic activity. The Zener double exchange mechanism is feasible in the oxide due to the existence of multiple valence (Co^{2+}, Co^{3+}, and Co^{4+}) cobalt ions, resulting in this magnetic behaviour [1], [16].

The dielectric investigations of barium cobalt carbonate precursor and oxide powder pelletized using a hydraulic press technique with a pressure of 7 tonnes, resulting in a pellet with a diameter of 12 mm and a thickness of 1 mm. Electronic grade silver paints were used to finely polish the pellets. Calculate the dielectric constant (ε') using the formula (3)

$$\varepsilon' = ct/\varepsilon_0 A \tag{3}$$

$$\sigma_{ac} = \omega\varepsilon_0\varepsilon' tan\delta \tag{4}$$

$$\omega = 2\pi f \tag{5}$$

$$\sigma = \sigma_0\, exp\,(E_a / kT) \tag{6}$$

Where C is the capacitance calculated from the analysis, t is the pellet thickness, 0 is the free space permittivity, A is the pellet area, and f is the applied ac. The Boltzmann constant is k, and the temperature is T [17]. The formula for calculating ac conductivity (4, 5 & 6). The activation energy was calculated using the graph ac vs. inverse temperature in kelvin.

At room temperature, the dielectric constant (ε) of $BaCoO_{3-\delta}$ varies with frequency (Fig.10). The dielectric constant falls as the strong relaxation of' seen at the examined frequency increases, implying a relaxor-like activity. Weak interactions between the dipoles in the multilayer structure were blamed for this phenomenon [17]–[19] The presence of two types of charge carriers in carbonate and oxide, namely, p type, can be attributed to the conduction process as a hole exchange between Co^{3+} and Co^{2+} and O_2 transfer between the filled and unoccupied oxygen sides.

The mechanism can be explained using the following equations (7 and 8).

$$Co^{3+} \longrightarrow Co^{2+} + h^{*} \tag{7}$$

$$1/2O_2 + V^{2*} \longrightarrow O^{2-} \tag{8}$$

The frequency dependence of dielectric loss (or) tan also reduces with increasing frequency, as shown in Fig.11. With increasing frequency, the dielectric loss decreases until it reaches a point where it remains constant up to 5MHz. As a result of the stray capacitance, the loss increases. Due to the ordered motion of weakly bound charged particles, the frequency dependence of electrical conductivity diminishes for both precursor and oxide (Fig.12). Due to the space charge polarization conduction mechanism, charge carriers dominate the external field.

At a frequency of 5 kHz, Fig.13 illustrates the temperature dependence of ac for carbonate precursor and $BaCoO_{3-\delta}$. As a result, studying electrical conductivity is crucial. As the temperature rises, the conductivity drops. The activation energies estimated using curve fitting equation (6) show that the crystal's activation energy is less than 1eV. Because of the involvement of space charge, the low activation energy supports intrinsic conduction. Between the sample and the electrode, a space charge is produced [20]–[22].

E_a = 0.6eV is the activation energy obtained using curve fitting. Due to the participation of space charge carriers and holes in the carbonate precursor and oxide material, the low activation energy supports intrinsic conduction. This demonstrates how carbonate and its oxide substance transmit electricity.

The resistivity of $BaCoO_{3-\delta}$ is measured in Fig.14. The ceramic $BaCoO_{3-\delta}$ sample was crushed into a 12mm diameter pellet and sintered for 12 hours at 800°C. The pellet was utilized as a sample for electrical resistivity testing using the four-probe method, with an applied current (I) of 8 mA and a temperature range of 300-473K. The approach is best suited for low and precise resistance measurements because it eliminates the consequences of sample-to-electrical contact resistance connections[23]. The material's resistivity is calculated using the equation (9).

$$\rho = 2\pi S\, V/I \tag{9}$$

where S represents the probe distance (S=0.1875), V represents the voltage collected across the two inner contacts, and I represents the current flowing through the sample. The relationship between material resistivity and temperature is seen in Figure 14.

The electrical resistivity's temperature dependency demonstrates semiconducting nature. At room temperature, the valence and conduction bands must have a small number of charge carriers, hence the $BaCoO_{3-\delta}$ n-type semiconductor must have a large band gap. $BaCoO_{3-\delta}$ had the highest electrical resistance (0.80cm), which was reduced to 0.76cm when the temperature was raised from 300K to 473K. Thermal agitation occurs as the temperature rises, and some valence electrons attain energy larger than Ea, jumping to the conduction band. The material's activation energy is computed using the equation (10), where k is the Boltzmann constant.

$$E_a = (2.303 \times 2k \times slope)/2 \tag{10}$$

The graph shown between log10 versus T-1 in Fig.15 demonstrates that at room temperature, the electrical resistivity is larger, but as the temperature rises, the resistivity reduces due to the hopping conduction process. The activation energy of $BaCoO_{3-\delta}$ is 0.6eV, and the slope value is determined from the graph and substituted in equation (10). This demonstrates how carbonate and its oxide substance transmit electricity.

4. Conclusion

Preparation of $BaCoO_{3-\delta}$ using the co-precipitation barium cobalt carbonate precursor method. The temperature of single-phase formation of oxide is 900°C, according to the phase formation temperature determined by thermal analysis. The scanning electron microscopy investigations shows the agglomerated spheres have an average grain size of 140 to 250 nm. The stoichiometry of the product $BaCoO_{3-\delta}$ was in good agreement with the elemental analysis by EDX and thermal analysis. Due to ligand to metal charge transfer, the optical band gap for carbonate precursor at 4eV acts as an insulating material. $BaCoO_{3-\delta}$ at 2eV behaves as an n-type semiconducting material. Carbonate to oxide materials that are anisotropic have their moment aligned in one direction of spontaneous magnetization and exhibit superparamagnetic activity. The findings show that the precursor method is a viable strategy for production of semiconducting cobalt-based perovskite material.

References

[1] G. Zvejnieks, D. Zavickis, E. A. Kotomin, and D. Gryaznov, "BaCoO3 monoclinic structure and chemical bonding analysis: hybrid DFT calculations," *Phys. Chem. Chem. Phys.*, vol. 23, no. 32, pp. 17493–17501, 2021, doi: 10.1039/D1CP01900G.

[2] M. Kauffmann, G. Ehora, S. Daviero-minaud, F. Abraham, and P. Roussel, "Structure , dimensionality and magnetism of new cobalt oxyhalides," vol. 10, pp. 471–475, 2008, doi: 10.1016/j.solidstatesciences.2007.12.032.

[3] A. J. J. and J.L.Hutchison, "An investigation of the structure of 12HBaCoO2.6 by electron microscopy and powder neutron diffraction," *J. Solid State Chem.*, vol. 35, pp. 334–340, 1980.

[4] G. Ehora, C. Renard, S. Daviero-Minaud, and O. Mentré, "New BaCoO3-δ Polytypes by Rational Substitution of O2- for F-," *Chem. Mater.*, vol. 19, no. 12, pp. 2924–2926, Jun. 2007, doi: 10.1021/cm070576o.

[5] B. E. Gushee, L. Katz, and R. Ward, "The Preparation of a Barium Cobalt Oxide and other Phases with Similar Structures1,2," *J. Am. Chem. Soc.*, vol. 79, no. 21, pp. 5601–5603, Nov. 1957, doi: 10.1021/ja01578a004.

[6] P. M. Botta, V. Pardo, C. de la Calle, D. Baldomir, J. A. Alonso, and J. Rivas, "Ferromagnetic clusters in polycrystalline BaCoO3," *J. Magn. Magn. Mater.*, vol. 316, no. 2, pp. e670–e673, 2007, doi: https://doi.org/10.1016/j.jmmm.2007.03.058.

[7] K. Conder, E. Pomjakushina, A. Soldatov, and E. Mitberg, "Oxygen content determination in perovskite-type cobaltates," *Mater. Res. Bull.*, vol. 40, no. 2, pp. 257–263, 2005, doi: https://doi.org/10.1016/j.materresbull.2004.10.009.

[8] Q. Shen, Z. Shao, S. Li, G. Yang, J. Yuan, and X. Pan, "Experimental Study of O2-Enriched CO2 Production by BaCo0.8B0.2O3−δ (B=Ce, Al, Fe, Cu) Perovskites Sorbent for Marine Exhaust CO2 Capture Application," *J. Mar. Sci. Eng.*, vol. 9, no. 6, 2021, doi: 10.3390/jmse9060661.

[9] S. Lin *et al.*, "A Photostimulated BaSi 2 O 5 :Eu 2+ ,Nd 3+ Phosphor-in-Glass for Erasable-Rewritable Optical Storage Medium," *Laser Photonics Rev.*, vol. 13, no. 4, pp. 1–11, 2019, doi: 10.1002/lpor.201900006.

[10] B. Liu, J. Sunarso, Y. Zhang, G. Yang, W. Zhou, and Z. Shao, "Highly Oxygen Non-Stoichiometric BaSc0.25Co0.75O3-δ as a High-Performance Cathode for Intermediate-Temperature Solid Oxide Fuel Cells," *ChemElectroChem*, vol. 5, no. 5, pp. 785–792, 2018, doi: https://doi.org/10.1002/celc.201701309.

[11] C. M. Holl, J. R. Smyth, H. M. S. Laustsen, S. D. Jacobsen, and R. T. Downs, "Compression of witherite to 8 GPa and the crystal structure of BaCO3II," *Phys. Chem. Miner.*, vol. 27, no. 7, pp. 467–473, 2000, doi: 10.1007/s002690000087.

[12] K. Vidyasagar, J. Gopalakrishnan, and C. N. R. Rao, "A convenient route for the synthesis of complex metal oxides employing solid-solution precursors," *Inorg. Chem.*, vol. 23, no. 9, pp. 1206–1210, Apr. 1984, doi: 10.1021/ic00177a008.

[13] A. Jada, S. Ladhari, and K. Jradi, "Synthesis of {BaCO}3 particles tailored by carboxylated cellulose fibers," *{IOP} Conf. Ser. Mater. Sci. Eng.*, vol. 827, p. 12008, Jun. 2020, doi: 10.1088/1757-899x/827/1/012008.

[14] A. Klinbumrung, A. Phuruangrat, T. Thongtem, and S. Thongtem, "Synthesis, Characterization and Optical Properties of BaMoO4 Synthesized by Microwave Induced Plasma Method," *Russ. J. Inorg. Chem.*, vol. 63, no. 6, pp. 725–731, 2018, doi: 10.1134/S0036023618060141.

[15] H. I. Antao S M, "THE ORTHORHOMBIC STRUCTURE OF CaCO3, SrCO3, PbCO3 AND BaCO3: LINEAR STRUCTURAL TRENDS," *Can. Mineral.*, vol. . 47, pp. 1245–1255, 2009.

[16] Y. Y. Chin *et al.*, "PHYSICAL REVIEW B 100 , 205139 (2019) Spin-orbit coupling and crystal-field distortions for a low-spin 3 d 5 state in BaCoO 3," vol. 205139, pp. 1–11, 2019, doi: 10.1103/PhysRevB.100.205139.

[17] B. Lal, K. K. Bamzai, P. N. Kotru, and B. M. Wanklyn, "Microhardness, fracture mechanism and dielectric behaviour of flux-grown GdFeO 3 single crystals," *Mater. Chem. Phys.*, vol. 85, no. 2–3, pp. 353–365, 2004, doi: 10.1016/j.matchemphys.2004.01.013.

[18] A. L. Kholkin, M. Avdeev, M. E. V Costa, J. L. Baptista, and S. N. Dorogovtsev, "Dielectric relaxation in Ba-based layered perovskites," *Appl. Phys. Lett.*, vol. 79, no. 5, pp. 662–664, Jul. 2001, doi: 10.1063/1.1386616.

[19] N. Rezlescu and E. Rezlescu, "Abnormal dielectric behaviour of copper containing ferrites," *Solid State Commun.*, vol. 14, no. 1, pp. 69–72, 1974, doi: https://doi.org/10.1016/0038-1098(74)90234-8.

[20] H. M. Zaki, "AC conductivity and frequency

dependence of the dielectric properties for copper doped magnetite,” *Phys. B Condens. Matter*, vol. 363, no. 1, pp. 232–244, 2005, doi: https://doi.org/10.1016/j.physb.2005.03.026.

[21] D. Szwagierczak and J. Kulawik, “Influence of MnO2 and Co3O4 dopants on dielectric properties of Pb(Fe2/3W1/3)O3 ceramics,” *J. Eur. Ceram. Soc.*, vol. 25, no. 9, pp. 1657–1662, 2005, doi: https://doi.org/10.1016/j.jeurceramsoc.2004.05.022.

[22] C.-C. Huang, D. P. Cann, X. Tan, and N. Vittayakorn, “Phase transitions and ferroelectric properties in BiScO3-Bi(Zn1⁄2Ti1⁄2)O3-BaTiO3 solid solutions,” *J. Appl. Phys.*, vol. 102, no. 4, p. 44103, Aug. 2007, doi: 10.1063/1.2769787.

[23] Y. SINGH, “ELECTRICAL RESISTIVITY MEASUREMENTS: A REVIEW,” *Int. J. Mod. Phys. Conf. Ser.*, vol. 22, pp. 745–756, Jan. 2013, doi: 10.1142/S2010194513010970.

Table captions

Table-1. A comparison of the magnetic behavior of carbonate precursor and $BaCoO_{3-\delta}$ oxide at ambient temperature

Barium cobalt carbonate precursor	**$BaCoO_{3-\delta}$ oxide product**
Magnetic saturation (**M_s**=9.87x10^{-3} emu)	Magnetic saturation (**M_s**=7.9x10^{-3} emu)
Magnetic retentivity (**M_r** =15.16x10^{-6}emu)	Magnetic retentivity (**M_r** =15.36x10^{-6}emu)
Magnetic coercivity (**H_c**=14.72G)	Magnetic coercivity (**H_c**=28.50G)

Figure captions

Figure.1. Thermal analysis of barium cobalt carbonate precursor to $BaCoO_{3-\delta}$ oxide

Figure.2. XRD patterns of carbonate precursor and $BaCoO_{3-\delta}$

Figure.3. SEM image of barium cobalt carbonate precursor and $BaCoO_{3-\delta}$

Figure.4. EDX elemental composition of $BaCoO_{3-\delta}$

88

Figure.5. FTIR spectra of carbonate precursor and $BaCoO_{3-\delta}$

Figure.6. FT-Raman spectra of precursor and $BaCoO_{3-\delta}$

Figure.7. Carbonate precursor and $BaCoO_{3-\delta}$ - UV-reflectance spectrum

Figure.8. UV-DRS band gap of carbonate precursor and $BaCoO_{3-\delta}$

Figure.9. Magnetic moment vs. Field for carbonate precursor and $BaCoO_{3-\delta}$

Figure.10. Dielectric constant versus log F for carbonate precursor and $BaCoO_{3-\delta}$

Figure.11. Dielectric loss versus log F for carbonate precursor and $BaCoO_{3-\delta}$

Figure.12. Electrical conductivity (σ) versus log F for carbonate precursor and $BaCoO_{3-\delta}$

Figure.13. Variation of electrical conductivity (σ) as a function of temperature for carbonate precursor and $BaCoO_{3-\delta}$

Figure.14. Electrical resistivity (ρ) as a function of temperature for $BaCoO_{3-\delta}$

Figure.15. $\log_{10}\rho$ versus 1000T^{-1} to calculate the activation energy

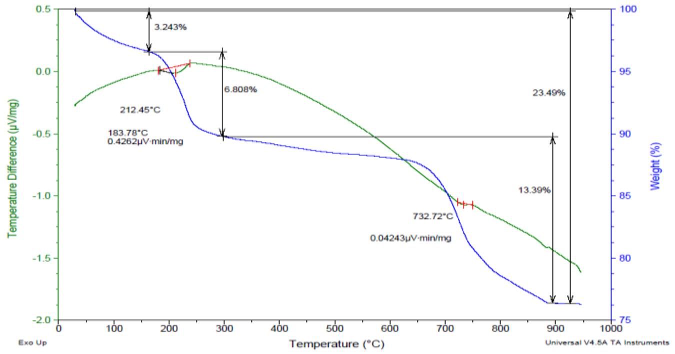

Figure.1.

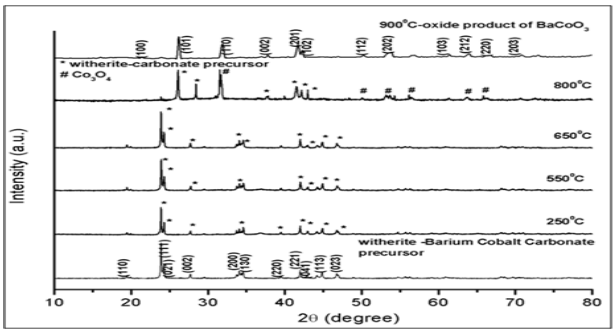

Figure.2.

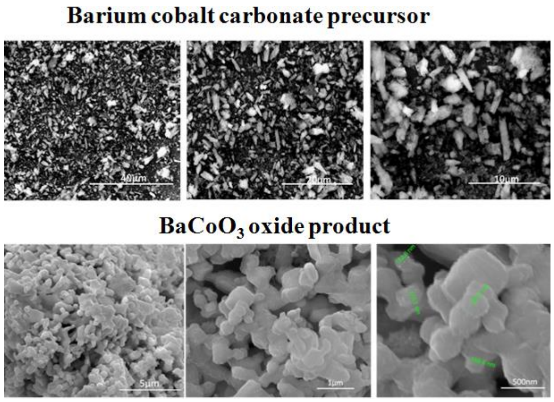

Figure.3.

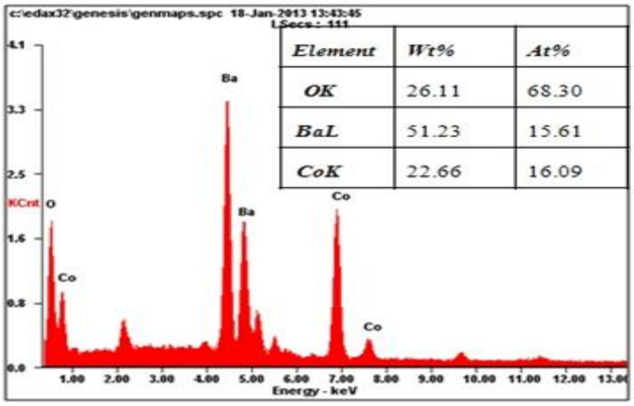

Element	Wt%	At%
OK	26.11	68.30
BaL	51.23	15.61
CoK	22.66	16.09

Figure.4.

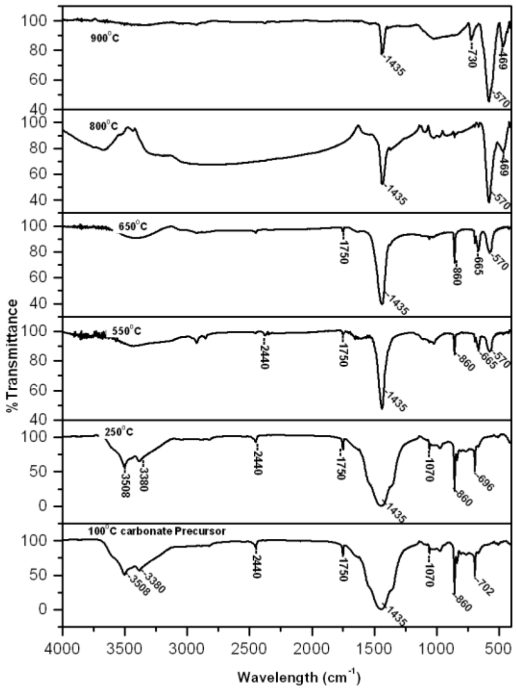

Figure.5.

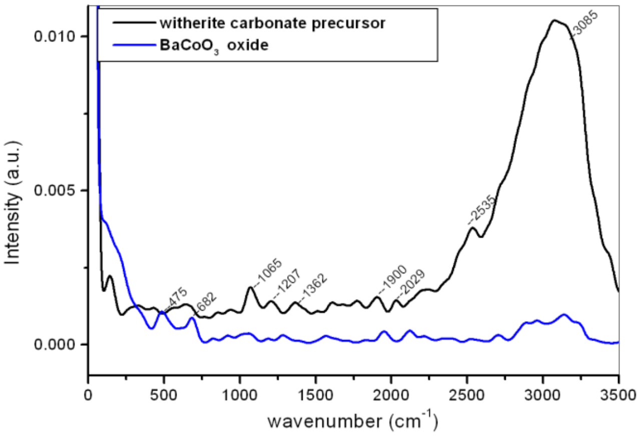

Figure.6.

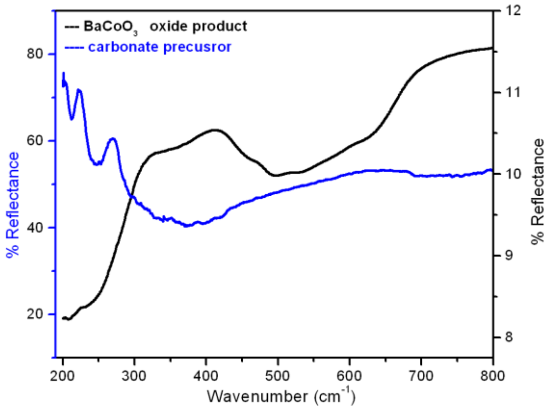

Figure.7.

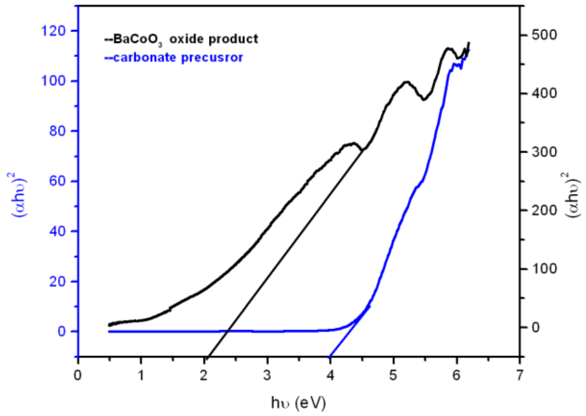

Figure.8.

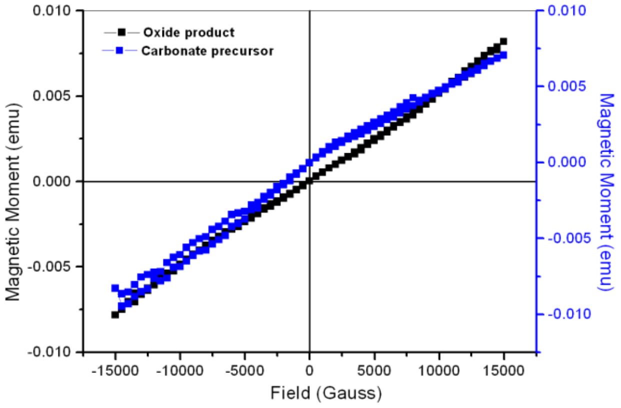

Figure.9.

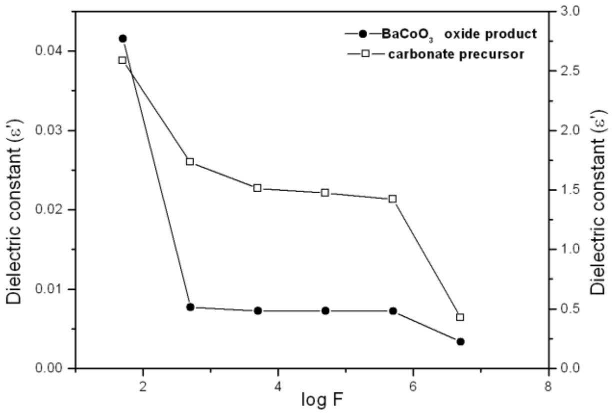

Figure.10.

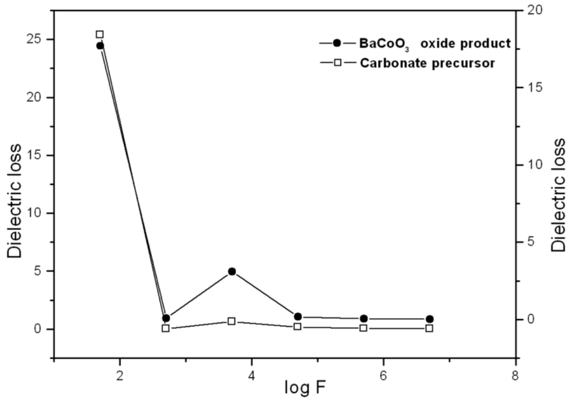

Figure.11.

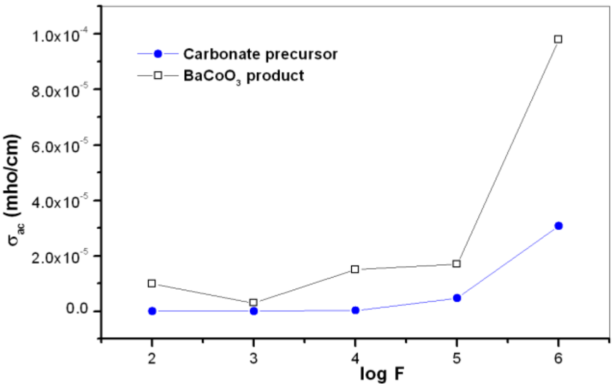

Figure.12.

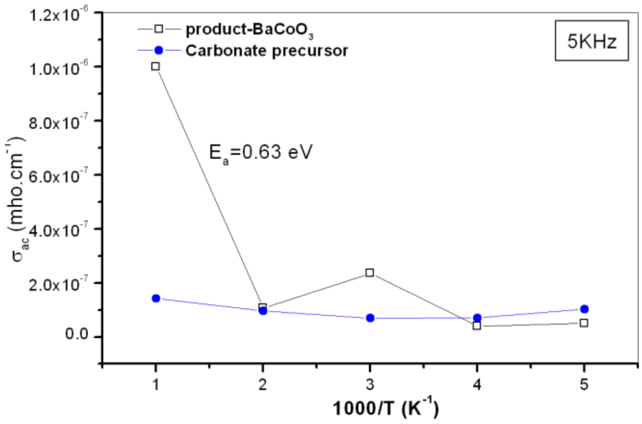

Figure.13.

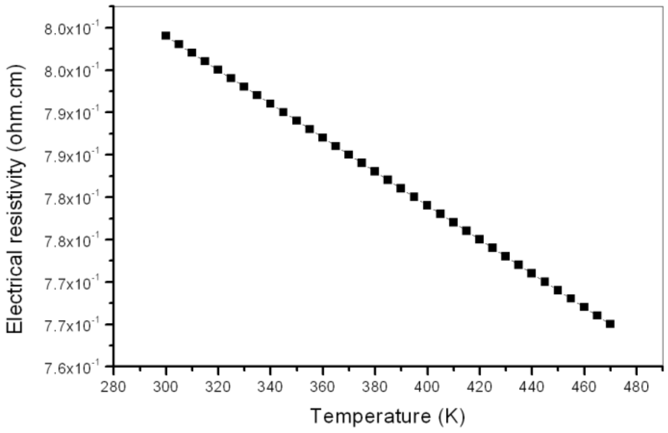

Figure.14.

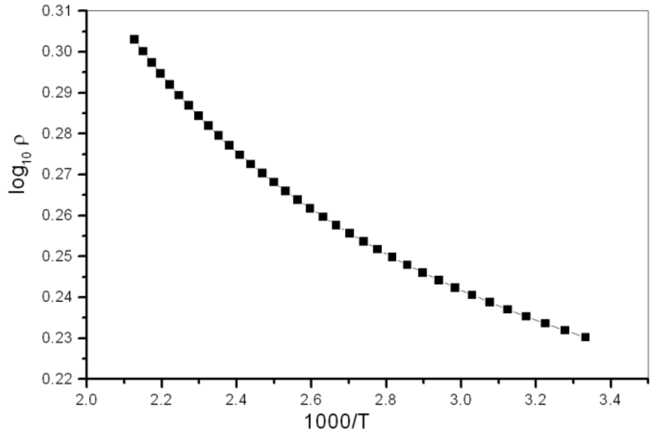

Figure.15.